Chalcogenide Letters Vol. 17, No. 12, December 2020, p. 593 - 603

SYNTHESIS OF CHALCOPYRITE $CuInSe_2$ (CIS) NANOSHEETS USING VITAMIN C AS AN ADJUVANT AND PHOTOELECTRIC PROPERTIES OF CIS THIN FILMS

X. L. CHEN[a], Y. M. ZHANG[a], J. F. WAN[b], J. L. DU[a], Z. L. ZHAO[a], G. WANG[a,b,c,*]
[a]*College of Physics and Electronic Information Engineering, Qinghai University for Nationalities, Xining 810007, China*
[b]*Key College of Chemistry and Chemical Engineering, Qinghai Nationalities University, Xining 810007, China*
[c]*Key Laboratory of Resource Chemistry and Ecological Environment Protection of the Qinghai Tiber Plateall, Qinghai University for Nationalities, Xining 810007, China*

To prepare chalcopyrite-phase $CuInSe_2$ (CIS) nanosheets, green reductants were screened by using them to reduce the valence state of copper sources using a *N*,*N*-dimethylformamide/triethylene glycol(DMF/TEG) mixed solvent. CuCl was used as the copper source, indium chloride as the indium source, selenium powder as the selenium source, TEG as the anionic solvent, DMF as the cationic solvent, and Vitamin C (Vc) as the reductant. The influences of reaction temperature, reaction time, and Vc amount on the phase and composition of synthetic $CuInSe_2$ nanosheets were examined, and the results were used to propose a reaction mechanism. The optional reaction conditions were a reaction temperature of 260 ^oC, a reaction time of 16 h, and a Vc amount of 0.20 g. Chalcopyrite-phase CIS nanosheets were synthesized with particle sizes of 14 μm and a uniform particle size distribution. $CuInSe_2$ thin films displayed good surface smoothness and compactness in a 5.5 μm spin-cast film. The thin film showed a bandgap of 1.08 eV, a carrier concentration of 5.26×10^{16} cm^{-3}, and a carrier mobility of 150.41 cm^2 V^{-1} S^{-1}. The results showed that this strategy can be used to prepare chalcopyrite-phase CIS which could be used as a photosensitive layer for various optoelectronic devices.

(Received October 8, 2020; Accepted December 2, 2020)

Keywords: Synthesis, Solvothermal method, $CuInSe_2$, Thin films, Photoelectric properties

1. Introduction

CIS is a direct band gap semiconductor with a high light absorption coefficient[1], whose band gap can be adjusted through doping with Ga[2], Al[3], S[4], and other elements[5, 6]. It has been widely used in CIS-based thin-film solar cells[7-9], QD solar cells[10-12], DSSCs solar cells[12], and photodetectors[13]. As the core material of many photoelectric devices, CIS is the parent material for the preparation of quaternary compounds[14]. Thus, there is a need for a simple

* Corresponding author: wang_gang_1001@163.com

and green method to synthesize chalcopyrite-phase CIS materials because this phase has a higher light absorption coefficient, is stable, and provides protection against incident radiation[15]. Among the CIS synthesis methods, liquid-phase synthesis been investigated[16-20] due to its ability to control chemical composition ratios, simple doping process, and low preparation environment requirements.

Solvothermal methods for synthesizing CIS-based compounds mainly include hot injection and microwave solvothermal methods. Badgujar et al[21]. used the microwave solvothermal method with copper nitrate as the copper source and triethanolamine as the solvent to synthesize $CuIn_{0.7}Ga_{0.3}Se_2$ nanosheets, but they did not report a reaction temperature. He et al[22]. used a thermal injection method, with copper(II) acetylacetonate as the copper source, tri-*n*-octylphosphine oxide (TOPO) as the solvent, and oleylamine as the adjuvant, to synthesize $Cu_2ZnSn\ (S,Se)_4$ quantum dots at 325 ^oC. Houck et al[23].used a hot injection method, with CuCl as the copper source, diphenylphosphine as the solvent, and oleylamine as the adjuvant, to synthesize $CuIn_xGa_{1-x}Se_2$ nanocrystals at 240 ^oC. Jia et al[24].used a hot injection method, with copper acetate as the copper source, trioctylphosphine as the solvent, and oleic acid as the adjuvant, to synthesize $CuInSe_2$ nanowires at 360 ^oC. Zhu et al[25].used a solvothermal method, with copper acetate as the copper source and dimethylformamide as the solvent, to synthesize $CuInSe_2$ nanosheets with poor crystallinity and impurities. Xu et al[26]. synthesized $Cu_{2-x}Se$ using copper nitrate as the copper source. They then used $Cu_{2-x}Se$ to prepare CuSe in an acidic solution to obtain $CuInSe_2$ nanowires using TEG as the solvent by a Solvothermal method at 200 ^oC.

The above synthesis methods all have strict requirements for solvents, reductants, and reaction temperatures. When used as the copper source, Cu^{2+} not only requires a relatively strong adjuvant but also requires a reaction temperature of 300 ^oC or higher. In contrast, Cu^+ requires a lower reaction temperature. Cu^{2+} must be reduced Cu^+, which requires a stronger reductant or a higher reaction temperature in order to increase the reducibility of the solvent. Although the need for a strong reducibility and a high reaction temperature can be lowered using Cu^+ as the copper source, the reaction temperature still exceeds 230 ^oC. Additionally, Cu^+ is mostly insoluble in high-boiling-point solvents such as alcohols, but it is soluble in solvents with lower boiling points such as formamides. However, the low boiling points of these solvents prevent them from being used in high-temperature reactions. Other suitable solvents are toxic and harmful and cause environmental pollution[2, 23, 25]. As a result, there are no suitable green solvents with high boiling points that can dissolve Cu^+. Additionally, the reductants used for both Cu^{2+} and Cu^+ are mostly toxic and harmful reductants, such as hydrazine hydrate[12], oleylamine[27], oleic acid[23], and ethylenediamine[28], which results in a preparation process that can easily cause environmental pollution.

Here, we aim to dissolve Cu^+ in a high boiling point green solvent and remove the traditional toxic and harmful reductants. Vitamin C was screened as a green reducing agent by using it to reduce copper sources. The use of Cu^+ as the copper source led to lower requirements on the strength of reducing agents during the chemical reaction. We also investigated the use of a blended solvent of DMF and TEG to dissolve the monovalent copper source and improve the yield of target products. The proposed solution was used to realize the all-green synthesis of chalcopyrite CIS nanosheets, and a mechanism for the chemical synthesis was proposed. Finally, the photoelectric properties of the products were determined by preparing and characterizing thin films.

2. Experimental

2.1. Chemicals

Copper(I) chloride (CuCl 97%), indium(III) chloride ($InCl_3$•$4H_2O$, 99.9%), selenium powder (Se, 99.9%), polyvinylpyrrolidone (PVP, M_w = 58,000), vitamin C (Vc, 98%), *N*,*N*-dimethylformamide (DMF, 98%), absolute ethanol (C_2H_5OH, 99.99%), and triethylene glycol (TEG, 98%) were purchased from Aladdin and used as received without further processing.

2.2. Synthesis of CIS nanosheets

Fig. 1 shows a schematic of the synthesis of CIS. The cationic precursor solution was prepared by adding 5 ml of DMF, 1 mmol of CuCl, and 1 mmol of $InCl_3 \cdot 4H_2O$ to a 10 ml beaker filled with magnets. The beaker was sealed with a heat-sealing film and moved to a magnetic stirrer and stirred at room temperature for 30 min at 300 rpm.

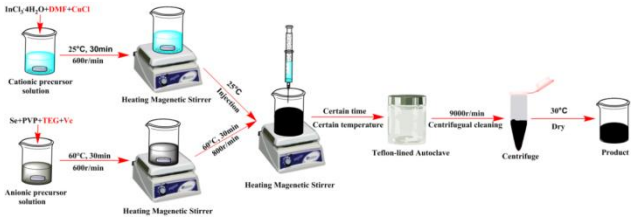

Fig. 1. Schematic diagram of the synthesis of CIS.

Then, 25 ml of TEG, 2 mmol of selenium powder, and 0.10 g of PVP were added to a 50 ml beaker filled with magnets. The beaker was sealed with a heat sealing film, and the beaker was moved to a magnetic stirrer in a 60 ^oC water bath and stirred for 30 min at 300 rpm. After the anionic precursor solution was prepared, it was injected into the cationic precursor solution and stirred at 60 ^oC. After stirring for 3 min at 500 rpm, the anionic precursor solution was fully mixed with the cationic precursor solution. Finally, the fully mixed solution was added to a 50 ml polytetrafluoroethylene reactor that was then moved into a muffle furnace. The solution was reacted for a specific time, and the temperature was raised to a specific reaction temperature at a ramp rate of 10 ^oC/ min. Then, the reactor was taken out when the temperature decreased to 25 ^oC at a temperature decrease rate of 10 ^oC/min. The solution in the reactor was removed and then washed with anhydrous ethanol in a centrifuge (TG16G, Tianjin Guangfeng Science and Technology Co., Ltd.) for 5 times at a speed of 9000 rpm for 10 min. After being washed, the product was dried in a drying box at 30 ^oC.

2.3. Preparation of CIS thin films

First, the synthesized CIS was prepared into a spin-coating solution with a concentration of 0.05 g/ml in anhydrous ethanol and ultrasonically dispersed for 40 min at a frequency of 40 kHz, a temperature of 30 ^oC, and a power of 300 W. Then, the FTO conductive glass (5×5 cm^2) was ultrasonically cleaned with acetone and absolute ethanol and then dripped into the spin coating solution. It was accelerated to 150 rpm by a spin coater (MSC-400B, Mycro Technologies) at an acceleration rate of 10 r/min^2 for 3 min. Finally, the conductive glass was transferred to a hot plate

(ZRX-27785, Beijing Zhongruixiang Technology Co., Ltd.) and baked at 30 ^{o}C for 5 min. The above process was repeated 3 times. After the films were prepared, the film and 0.2 g of selenium powder were added into a tubular furnace with a 6 × 100 cm^2 quartz tube. The temperature was raised to 550 ^{o}C at a heating rate of 5 ^{o}C/min, and selenylation was carried out at this temperature for 30 min under Ar gas protection at a flow rate of 0.15 L/min.

2.4. Materials characterization

XRD patterns were obtained using an X-ray powder diffractometer (XRD, Bruker D8 Advanced, Germany) with Cu *K*α radiation at 40 kV and 40 mA. The microstructures and element content of the products were characterized using scanning electron microscope (SEM, JSM 7800F, Japan), transmission electron microscopy (TEM, JEM 2100F, Japan) and their respective energy-dispersive spectroscopy. The bonding states of the synthesized products were analyzed by Raman spectrometer (Renishaw in Via reflex, England) with 532 nm laser wavelength. The UV-Vis-NIR spectra of $CuInSe_2$ thin films from 400 nm to 1500 nm were collected with a UV-Vis–NIR spectrophotometer (UV-3600, Shimadzu, Japan). Hall measurements were performed using a physical property measurement system (PPMS, Quantum Design PPMS-9, America).

3. Result and discussion

3.1. Effect of reaction temperature on synthesis

When using 0.20 g Vc and a 12 h reaction time, the influence of reaction temperature on the phase composition of the product was explored. The experimental results are shown in Fig. 2. Fig. 2 is an XRD pattern of the product obtained at different reaction temperatures. When the reaction temperature was 200 ^{o}C, the diffraction pattern contained strong diffraction peaks at 2θ = 26.57°, 44.23°, and 52.39°, which is consistent with the main characteristic diffraction peaks of the (112), (220), and (312) crystal planes of chalcopyrite-phase $CuInSe_2$ (JCPDS: 40-1487). The three weak diffraction peaks at 2θ = 26.75°, 44.60°, and 52.91° were consistent with the main characteristic diffraction peaks of the (200), (220), and (311) crystal planes of $Cu_{2-x}Se$ (06-0680). There were weak diffraction peaks at 2θ = 28.11°, 31.10°, 46.05°, and 50.01°, which were consistent with the main characteristic diffraction peaks of the (102), (006), (110), and (108) crystal planes of CuSe (JCPDS: 34-1071). Therefore, when the reaction temperature was 200 ℃, the main phase component in the synthesized product was chalcopyrite-phase $CuInSe_2$ (JCPDS: 40-1487). There were also two impurity phases of $Cu_{2-x}Se$ (JCPDS: 06-0680) and CuSe (JCPDS: 34-1071). When the reaction temperature was raised to 230 ^{o}C, the characteristic diffraction peaks of $CuInSe_2$ and CuSe strengthened, but the characteristic diffraction peak of $Cu_{2-x}Se$ weakened. Quantitative analysis showed that when the reaction temperature was 230 ^{o}C, the relative content of $CuInSe_2$ and CuSe in the product increased, while the relative content of $Cu_{2-x}Se$ decreased. When the reaction temperature was increased to 260 ^{o}C, the characteristic diffraction peaks of $Cu_{2-x}Se$ and CuSe completely disappeared, and weak diffraction peaks appeared at 2θ = 27.68°, 30.87°, and 41.91°, which were the characteristic diffraction peaks of the (103), (200), and (105/213) crystal planes of CIS. Compared with the patterns of products obtained at 200 ^{o}C and 230 ^{o}C, the peak width of the main diffraction peaks was narrower, and the peak was sharper. This indicates that single-phase chalcopyrite $CuInSe_2$ with good crystallinity was prepared at 260 ^{o}C.

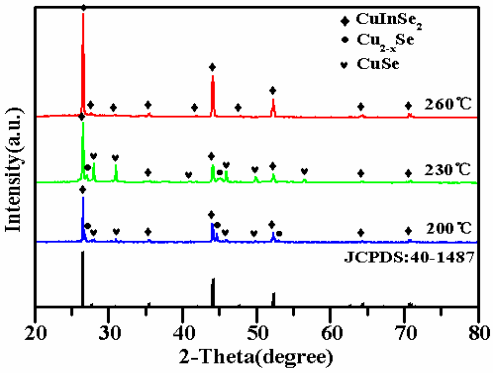

Fig. 2. XRD pattern of synthesized product at different reaction temperatures.

According to the above analysis, the reaction temperature has positive effects on the phase composition and crystallinity. An excessively low reaction temperature allows the formation of impurity phases in the target materials. Increasing the reaction temperature promoted the transformation between impurity-phase $Cu_{2-x}Se$ and CuSe-phase into $CuInSe_2$. The reason may be that increasing the reaction temperature can stimulate the reducibility of the solvent and the reductant. It especially made the solvent more sensitive to changes in the reaction temperature, and promoted the reduction of a large amount of selenium powder in a short time. At the same time, a higher temperature was more conducive to Ostwald ripening[29] and increased the crystallinity of the product.

3.2. Effect of reaction time on product synthesis

At a reaction temperature of 260 ^{o}C and 0.20 g Vc, the effect of reaction time on the phase composition of the product was investigated. The experimental results are shown in Fig. 3. Fig. 3 contains XRD patterns of the products obtained at different reaction times. When the reaction time was 4 h, according to the discussion in Section 3.1, the main phase of the product was chalcopyrite-phase $CuInSe_2$, with small amounts of $Cu_{2-x}Se$ and CuSe. When the reaction time was increased to 8 h, the characteristic diffraction peaks of $Cu_{2-x}Se$ and CuSe were greatly weakened, and the contents of the two impurity phases decreased upon increasing the reaction time.When the reaction temperature was increased to 12 h, the characteristic diffraction peaks of $Cu_{2-x}Se$ and CuSe completely disappeared, indicating that single-phase $CuInSe_2$ was obtained at 12 h reaction time. However, its peak was blunt, its half-peak width was broad, and its crystallinity was not good. After increasing the reaction time to 16 h, weak characteristic diffraction peaks of $CuInSe_2$ appeared at $2\theta = 27.68^{\circ}$ and 62.63° , and the half-width of the main diffraction peak decreased. This indicated that single-phase chalcopyrite CIS with good crystallinity was synthesized.

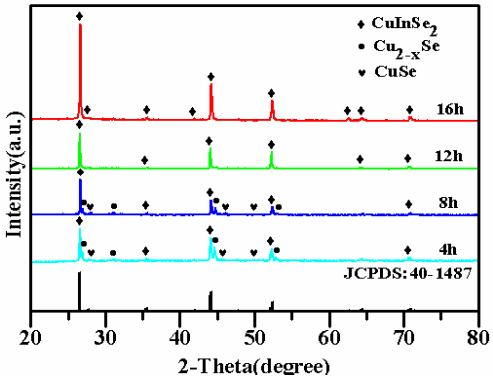

Fig. 3. XRD patterns of synthesized products at different reaction times.

According to the above analysis, it can be concluded that the influence of reaction time on the synthesized product had nearly the effect as that of the reaction temperature. It improved the crystallinity of the product. An insufficient reaction time resulted in the appearance of other impurity phases in the target product. Increasing the reaction also promoted the transformation of $Cu_{2-x}Se$ and CuSe to $CuInSe_2$. Extending the reaction time was have been conducive to the transformation of impurities to the target product and was conducive to Ostwald Ripening[29] of the original nucleated grains, which promoted the crystallinity of the product.

3.3. Effect of Vc dosage on product synthesis

Under a reaction temperature of 260 ^{o}C and a reaction time of 12 h, the effect of Vc dosage on the phase composition of the product was explored. The experimental results are shown in Fig. 4.

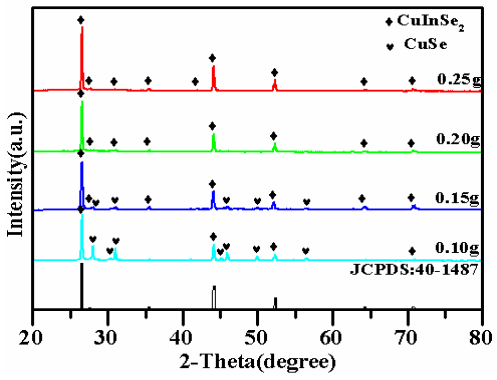

Fig. 4. XRD pattern of synthesized product at different Vc dosages.

Fig. 4 shows the XRD patterns of the products obtained at different Vc dosages. When the Vc dosage was 0.1 g, according to the discussion in Section 3.1, the main phase component was chalcopyrite $CuInSe_2$, with a small amount of CuSe but no $Cu_{2-x}Se$. When the dosage of Vc was 0.15 g, the characteristic diffraction peak of CuSe was weakened, indicating that its content was effectively reduced. When the dosage of Vc was 0.20 g, the characteristic diffraction peak of CuSe

completely disappeared, and the characteristic diffraction peak of $CuInSe_2$ increased, indicating the synthesis of pure $CuInSe_2$. When the amount of Vc was increased to 0.25 g, the diffraction peak intensity and half-peak width of the product were not different from those of 0.20 g Vc. This indicates that increasing the amount of Vc beyond 0.20 g has little effect on the phase composition and crystallinity of the product.

Based on the above discussion, it can be concluded that an appropriated dosage of Vc can effectively inhibit the production of CuSe impurities in the product and promote the synthesis of single-phase CIS. The main reason is that a higher Vc dosage served as a reducing agent during the chemical reaction so that there was enough reducing agent for the reduction of selenium powder in the later stages of the reaction. The reduced selenium ions promoted the transformation of impurities into target products.

3.4. Characterization of CIS nanosheets

According to the discussion in 3.1-3.3, the CIS compounds were synthesized under the optimal reaction conditions of a reaction temperature of 260 ^{o}C, a reaction time of 16 h, and a Vc amount of 0.25 g, and then the phase structure and composition of the synthesized products were characterized.

Fig. 5(a) shows the XRD spectrum of the product. It can be seen from the Figure that the diffraction peaks shape is sharp and the half peak width is narrower. In addition, there are relatively weak absorption peak at 2θ = 27.68. , 30.87. , 41.91. , 62.63. , and they correspond to the specific diffraction peaks of the chalcopyrite phase CIS at the crystal planes (103), (211), (105/321), (305/323), and (008), showing excellent crystallinity. Fig. 5(b) shows the SEM image of the product. It can be seen from the Figure that the morphology of the sample is nanosheets, and its particle size and thickness distribution are relatively uniform. The average particle size is about 14 um. However, there is a small amount of particle agglomeration. In order to further characterize the nanosheets, the products were tested by TEM. The test results are shown in Fig. 5(c) and (d). The planar morphology of the nanosheets is regular hexagonal, and the distance between the two diagonals is about 15 um. The HRTEM image of Fig. 5(d) indicates that the distances between the adjacent lattice fringes to be 0.33 nm, which corresponds with the (112) d-spacing for chalcopyrite-phase CIS, and agrees well with the XRD result. In addition, in order to further detect whether there were a very small amount of other impurities in the products, The bonding states and the relative contents of atoms of the products were analyzed by Raman spectrometer and energy-dispersive spectroscopy. It can be seen from the Raman spectra of Fig. 5(e) that a prominent peak at 174 cm^{-1}corresponding to the A1 mode of CIS , and there are faint peaks at 214cm^{-1} and 233cm^{-1}, corresponding to the A2 mode of CIS[30]. Fig. 5(f) is an EDS energy spectrum of a CIS compound. It can be seen that the relative contents of Cu, In and Se atoms in CIS compound are 23.23%, 24.79% and 51.98%, respectively. The atomic ratio of Cu, In and Se is 0.9:0.95:2, and the chemical formula formed is $Cu_{0.9}In_{0.95}Se_2$, which is highly close to the atomic ratio of CIS 1:1:2. Take together, these results indicate that the regular hexagonal chalcopyrite-phase CIS nanosheets with uniform particle size distribution and no other impurities were synthesized under the optimal experimental conditions.

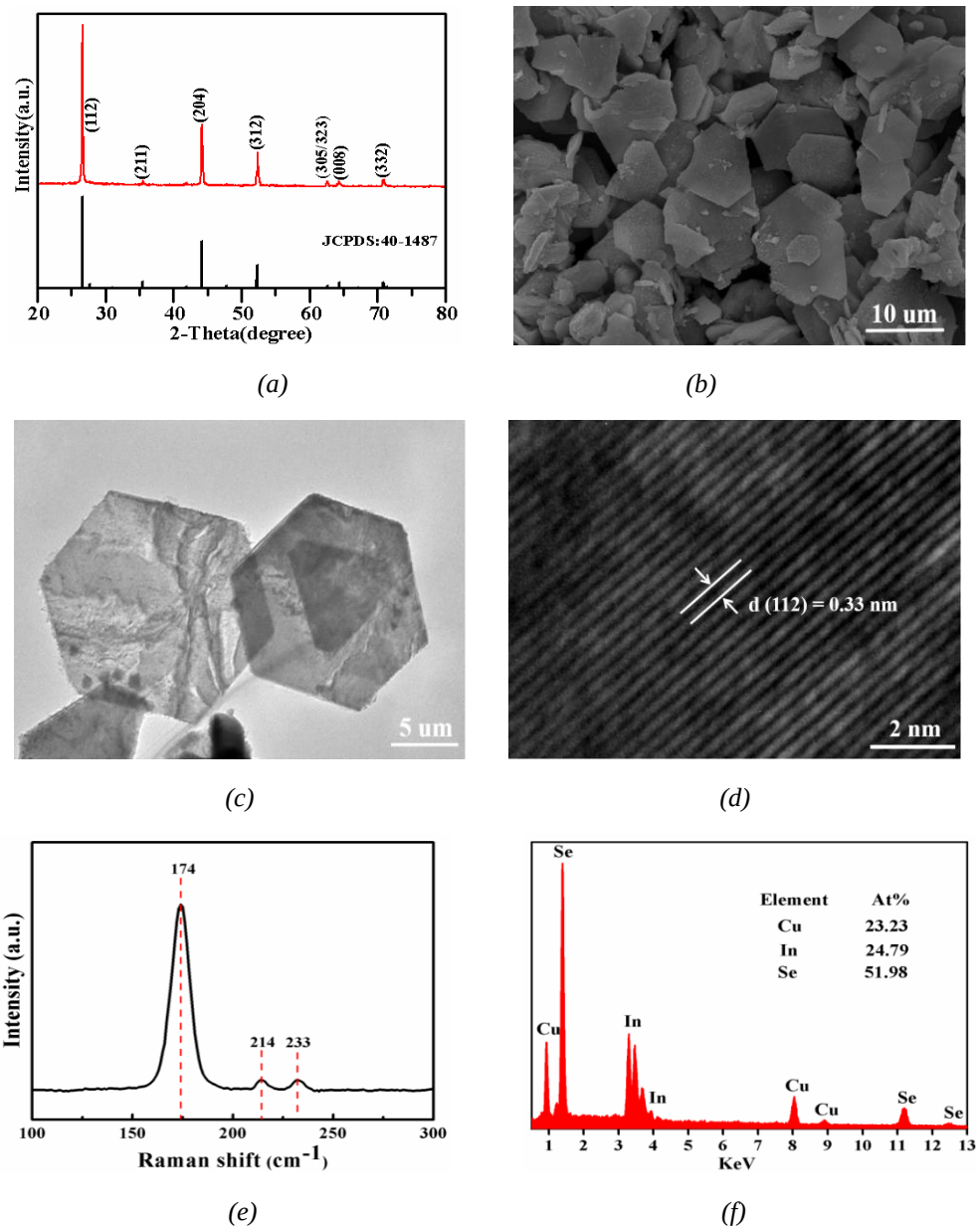

Fig. 5. XRD pattern(a), SEM image(b), TEM image(c), HRTEM image(d), EDS spectra(e) and Raman spectra(f) of CIS were Synthesized under optimal experimental conditions

3.5. Characterization of the structural properties and optical properties of thin films

CIS thin films were prepared by spin-coating and were selenized in a selenium atmosphere at 550 ^{o}C, and then the structural and photoelectric properties of the thin films were characterized.

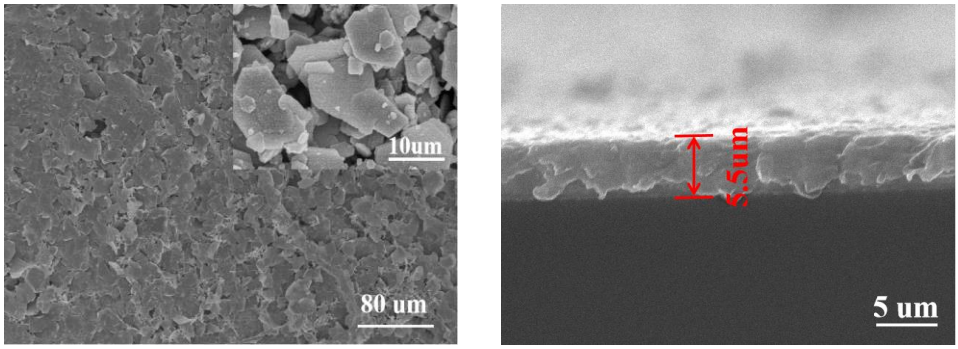

(a) *(b)*

Fig. 6. SEM images of the surface (a) and cross-section (b) of the film after selenylation

Fig. 6 (a) and (d) show are the SEM images of the surface and cross-sections after selenylation, respectively. As can be seen from Fig. 6 (a), the size of the nanosheets was about 14 μm, and their uniformity and dispersion were good. The flatness of the surface of the light absorption layer can improve the contact surface between the light absorption layer and the buffer layer, thus reducing leakage current, improving the built-in electric field, and eliminating carrier recombination centers. As can be seen from Fig. 6 (b), the compactness of the thin film after selenylation was improved, and its thickness was 5.5 μm.

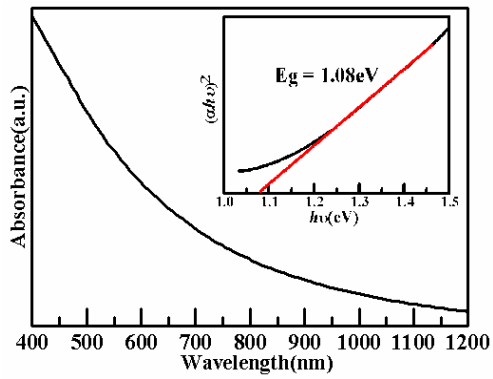

Fig. 7. The optical absorption spectrum and Tauc plot (inset) of a CIS film after selenylation.

Fig. 7 presents an ultraviolet-visible-near infrared fitted absorption spectrum of the CIS thin film. The absorption value of the prepared films increased slowly from 1200 – 900 nm, but increased sharply from 900 – 400 nm, which shows good absorption in both the visible and near-infrared regions. The inset of Fig. 7 is an illustration of $(\alpha h\nu)^2 - h\nu$ diagram converted from the absorption spectrum of the thin film. The linear portion of the $(\alpha h\nu)^2 - h\nu$ curve was extrapolated to the intersection point with an abscissa of 1.08. According to Tauc formula, the forbidden bandwidth of the CIS film was 1.08 eV, which conforms to the reported value of 1.06 eV[31] of CIS, but is slightly larger, possibly due to internal defects in the material.

Table 1. Electrical performance parameters of CIS thin films.

Conductivity	Electrical resistivity/Ω·cm	Carrier concentration/cm^{-3}	Carrier mobility/cm^2 V^{-1} S^{-1}
p	23.79	5.26×10^{16}	150.41

Table 1 shows the electrical performance parameters of the CIS thin films, which displays characteristics of a P-type semiconductor. Its carrier concentration, carrier mobility, and electrical resistivity are 5.26×10^{16} cm^{-3}, 150.41 cm^2 V^{-1} S^{-1}, and 23.79 Ω·cm, respectively, showing superior electrical performance and meeting the requirements for preparing high-efficiency CIS thin-film solar cell light absorption layers[28].

4. Conclusions

To prepare chalcopyrite-phase CIS, two strategies were adopted to screen the green reducing agent Vc by using it to reduce the copper source, and to use TEG/DMF as a blended solvent to realize the green synthesis of CIS. The effects of reaction time, reaction temperature, and Vc dosage on the phase and composition of the synthesized product were investigated by a solvothermal method. The results were used to propose a mechanism for the chemical reactions. CIS thin films were prepared by spin-coating, and the structural and photoelectric properties of the thin films were characterized.

The experimental results showed that under the optimal experimental conditions of a reaction temperature of 260 ^oC, an 18 h reaction time, and a 0.25 g Vc dosage, large flakes of CIS with a uniform particle size distribution of about 15 μm were prepared. The film has a smooth surface and a high degree of densification, with a thickness of 5.5 μm, a band gap of 1.08 eV, a carrier concentration of 5.26×10^{16} cm^{-3}, and a mobility of 150.41 cm^2 V^{-1} S^{-1}. It also displayed excellent optical and electrical properties. The results of this study show that the two preparation strategies can be used to prepare chalcopyrite-phase CIS that is suitable for preparing high-efficiency CIS thin films for solar cell light absorption layers.

Acknowledgements

The authors acknowledge the financial support from Key Natural Science Foundation of Qinghai province (2017-zj-729).

References

[1] K. L. Chopra, P. D. Paulson, V. Dutta, Prog. Photovolt: Res. Appl. **12**(23), 69 (2004).
[2] N. Oh, L. P. Keating, G. A. Drake, M. Shim, Chem. Mater. **31**(6), 1973 (2019).
[3] C. R. Dhas, A. J. Christy, R. Venkatesh, S. K. Panda, B. Subramanian, K. Ravichandran,

P. Sudhagar, A. M. E. Raj, J. Solid State Electrochem. **22**(8), 2485 (2018).
[4] W. Liu, D. B. Mitzi, M. Yuan, A. J. Kellock, S. J. Chey, O. Gunawan, Chem. Mater. **22**(3), 1010 (2010).
[5] K. Timmo, M. Altosaar, M. Pilvet, V. Mikli, M. Grossberg, M. Danilson, T. Raadik, R. Josepson, J. Krustok, M. Kauk-Kuusik, J. Mater. Chem. A **7**(42), 2428 (2019).
[6] T. Yan, Y. Li, X. Song, J. Wang, Z. Xie, D. Deng, J. Mater. Chem. C **7**(24)**,** 7279 (2019).
[7] U. Berner, D. Colombara, J. D. Wild, E. V. C. Robert, M. Schütze, F. Hergert, N. Valle, M. Widenmeyer, P. J. Dale, Prog. Photovolt: Res. Appl. **24**(6), 749 (2016).
[8] X. Huang, X. L. Chen, Z. W. Zhang, H. M. Ji, Y. L. Ma. Chalcogenide Letters **16**(11), 545(2019).
[9] S. Kim, M. S. Mina, J. Lee, J. Kim, ACS Appl. Mater. Interfaces **11**(49), 45702 (2019).
[10] C. Wang, D. Barba, H. Zhao, X. Tong, Z. Wang, F. Rosei, **11**(41), 19529 (2019).
[11] Y. Ma, Y. Zhang, W. W. Yu, J. Mater. Chem. C **7**(44), 13662 (2019).
[12] H. M. Daniel, N. Fuke, J. M. Pietryga, J. Phys. Chem. Lett. **4**(3), 355 (2013).
[13] M. G. Mali, H. Yoon, B. N. Joshi, H. Park, S. S. Al-Deyab, D. C. Lim, S. Ahn, C. Nervi, S. S. Yoon, ACS Appl. Mater. Interfaces **7**(38), 21619 (2015).
[14] S. M. Wasim, C. Rincón, G. Marín, J. M. Delgado, J. Contreras, J. Phys. D: Appl. Phys. **37**(3), 479 (2004).
[15] I. M. Kötschau, H. W. Schock, J. Phys. Chem. Solids **64**(10), 1559 (2003).
[16] Y. J. Song, J. Y. Kang, G. Y. Baek, J. A. Bae, S. H. Yang, C. W. Jeon, Prog. Photovolt: Res. Appl. **26**(3), 223 (2018).
[17] H. Guthrey, A. Norman, J. Nishinaga, S. Niki, M. Al-Jassim, H. Shibata, ACS Appl. Mater. Interfaces **12**(2), 3150 (2019).
[18] C. J. Pereyra, Y. D. Iorio, M. Berruet, M. Vazquez, R. E. Marotti, Phys. Chem. Chem. Phys. **21**(36), 20360 (2019).
[19] L. Zhang, H. Rao, Z. Pan, X. Zhong, ACS Appl. Mater. Interfaces **11**(44), 41415 (2019).
[20] X. L. Chen, X. J. Wang, X. Huang, Z. L. Zhao, L. Z. Bai, W. J. Liang, Y. L. Ma, Chalcogenide Letters **8**(17), 385 (2020).
[21] A. C. Badgujar, R. O. Dusane, S. R. Dhage, Mater. Sci. Semicond. Process **81**, 17 (2018).
[22] M. He, D. Kou, W. Zhou, Z. Zhou, Y. Meng, S. Wu, Inorg. Chem. **58**(19), 13285 (2019).
[23] D. W. Houck, S. V. Nandu, T. D. Siegler, B. A. Korgel, ACS Appl. Nano Mater. **2**(7), 4673 (2019).
[24] G. Jia, K. Wang, B. Liu, P. Yang, J. Liu, W. Zhang, R. Li, C. Wang, S. Zhang, J. Du, RSC Adv. **9**(61), 35780 (2019).
[25] Q. Zhu, W. Chen, F. Dai, Y. Yuan, X. Wu, J. Zai, R. Qi, X. Qian, ChemNanoMat. **1**(1), 52 (2015).
[26] J. Xu, C. S. Lee, S. T Lee, Y. B Tang, W. X. Zhang, X. Chen, Z. Yang, ACS Nano **4**(4), 1845 (2010).
[27] M. Ye, R. Tang, S. Ma, Q. Tao, X. Wang, Y. Li, P. Zhu, J. Phys. Chem. C **123**(34), 20757 (2019).
[28] R. Noufi, R. Axton, C. Herrington, S. K. Deb, Appl. Phys. Lett. **45**(6), 668 (1984).
[29] P. W. Voorhees, J. Stat. Phys. **38**, 231 (1985).
[30] K. G. Deepa, K. P. Vijayakumar, C. Sudhakartha, Mat. Sci. Semicon. Proc. **15**(2), 120 (2012).
[31] T. J. Whang, M. T. Hsieh, Y. C. Kao, S. J. Lee, Appl. Surf. Sci. **255**(8), 4600 (2009).